2022 IEEE Conference on Control Technology and Applications (CCTA)
August 22-25, 2022. Trieste, Italy

Robust MPC-based Synergy Control of a Hybrid Neuroprosthesis for Foot Placement

Krysten Lambeth, Ziyue Sun, Mayank Singh, Nitin Sharma*

Abstract—Multi-joint hybrid neuroprostheses provide therapeutic benefits for people with spinal cord injury, but they are typically overactuated, which makes input dimensional-ity reduction desirable. This can be done through artificial synergies that function like the biological synergies utilized by the human neuromuscular system. Bio-inspired synergistic control is here merged with a model predictive control (MPC) scheme for cooperative control of a hybrid neuroprosthesis that combines functional electrical stimulation (FES) with a powered exoskeleton. The controller assigns activation coefficients to artificial synergies to produce walking-like movement in a leg model that includes activation and muscle fatigue dynamics. The tube-based MPC scheme employs a sliding mode controller to ensure robustness and is formulated in task space to guide foot placement. The formulation is employed on a 2-degree of freedom hybrid neuroprosthesis model with 6 actuators.

I. Introduction

In 2020, the estimated population of persons living in the US with spinal cord injury totaled 294,000 [1]. The injury is often followed by muscle atrophy and bone loss, increasing the risk of fractures and metabolic complications [2]. There is evidence that functional electrical stimulation (FES) can assist in increasing muscle mass [3] as well as improving bone health [4], [5]. FES provides an electric current to a muscle while a functional action such as walking is performed. Recent studies of FES walking have demonstrated its facilitation of increased unassisted walking speed [6] and improved bone turnover [7] in patients with SCI, but FES-induced fatigue poses an obstacle to maximizing therapeutic benefit [8]. One method for reducing fatigue is the combination of a powered exoskeleton with FES. The exoskeleton decreases muscle demand and provides added torque for completing a motion, reducing fatigue as well as error [9]. Furthermore, a hybrid scheme reduces the power required by the exoskeleton motors [10] and improves kinematics in the presence of severe spasticity, a condition which can prevent exoskeleton use [11].

Hybrid FES-exoskeleton prostheses, or hybrid neuroprostheses (HNs), present a case of actuator redundancy; that is, the number of actuators exceeds the number of degrees of freedom (DOFs). A single joint can be actuated by an electric motor and stimulation of the extensor and flexor muscle groups. The control allocation problem has been addressed in multiple ways. In [12], separate controllers were designed for FES and motor inputs, and fatigue was minimized by applying FES only when an external disturbance was observed. Because this approach minimizes stimulation, however, the physiological benefits of FES may be limited. [10] maximized muscle contribution by using torque feedback to update FES such that it acted as a constructive disturbance to the PD motor controller, which was responsible for trajectory tracking. The design was applied to a 2-DOF HN with 2 actuators per joint. [13] used an allocation factor to distribute torque between FES and motor, updating the allocation factor to account for muscle fatigue. [14] implemented an iterative learning controller for a 2-DOF neuroprosthesis with 2 FES inputs per joint. For each joint, a single iterative learning controller determined the stimulation patterns for both muscle groups. [15] also looked at control of 2 FES muscle groups for a single joint. Modulated stimulation was sent to the extensors or flexors depending on deviation from the desired knee angle; however, both [14] and [15] addressed input dimensionality at the joint level rather than across joints, which may be desirable for higher-dimensional HNs. Other approaches avoid modulating FES and apply constant stimulation according to a timing law designed for a specific task [11], [16]. In [17], for example, predefined stimulation patterns were applied at specific times within the gait cycle, and the exoskeleton provided a set burst of torque at the start of each step.

An alternative method for addressing actuator redundancy is model predictive control (MPC). MPC is a form of constrained optimization that considers the state and control trajectories over a finite time horizon when determining the next control input; in other words, MPC considers future costs when choosing a solution. To address actuator redundancy, [18] used MPC for dynamic control allocation. Control was distributed between an electric motor and FES of the knee extensors, and the controller mitigated muscle fatigue by increasing motor demand. [19] used gradient projection MPC, and [20] employed tube-based MPC (TMPC), a robust MPC method that constrains inputs and terminal states within a specified region or "tube." [21] adapted TMPC for the nonlinear musculoskeletal dynamics, but only single-joint control was implemented in the aforementioned TMPC schemes.

K. Lambeth, Z. Sun, and N. Sharma are with the UNC/NC State Joint Department of Biomedical Engineering, NC State University, Raleigh, NC 27606 USA (e-mail: kflambet@ncsu.edu; zsun32@ncsu.edu; nsharm23@ncsu.edu). M. Singh is with the UNC State Department of Electrical and Computer Engineering, NC State University, Raleigh, NC 27606 USA (e-mail: msingh25@ncsu.edu). This work was funded by NSF Award #2124017.

*Corresponding author: Nitin Sharma. This work was funded by NSF Award #2124017.

2022 IEEE Conference on Control Technology and Applications (CCTA) | 978-1-6654-7338-5/22/$31.00 ©2022 IEEE | DOI: 10.1109/CCTA49430.2022.9966170

Another approach to the actuator redundancy problem is bio-inspired synergy control. The human spinal cord uses linear combinations of muscle activations, or muscle synergies, to perform complex motions [22]. Each synergy consists of a set of weights and an activation signal. It is the time-varying activation that is controlled in order to produce a given movement. The advantage of synergy control is that a few synergies can be used in place of a large number of actuators, potentially reducing computational burden. As opposed to natural synergies that recruit muscles, artificial synergies use FES and motors. For example, rehabilitative walking may be broken down into two dynamic postural synergies, so named because each produces a distinct posture. The first artificial synergy facilitates hip flexion, and the second produces knee extension [23]. This type of synergy control was accomplished in [24]. Synergy weights were extracted for a 4-link gait model with 9 actuators, and the gait model tracked a desired walking trajectory using only 2 synergies; however, the synergy activation signals were updated through a projection algorithm rather than assigned by optimization. Dynamic postural synergies were used in [25] with the added complexity of variable step length control. Non-robust MPC was used to allocate synergy activations without consideration of activation and fatigue dynamics.

The aim of this paper is to design a new robust TMPC scheme for allocating synergy activations to reduce actuator redundancy in a multi-joint lower-limb model that includes fatigue and activation dynamics. To the authors' knowledge, this is the first time TMPC has been combined with synergy control. Compared to single-joint TMPC, synergistic multi-joint control introduces additional design challenges as the actuator dynamics must be considered synergistically rather than individually and the torque contributions of motors and FES cannot simply be separated and summed. This problem is here addressed by creating a synergistic control law that serves as an input to the synergy activation signals rather than to the actuators themselves. Furthermore, whereas our previous work focused on joint angle tracking, this controller guides foot placement by considering task-space error. Task-space controllers are more intuitive for patients and therapists alike and can incorporate foot placement as a safety constraint [26]. This controller grants uniformly ultimately bounded stability against disturbances and modeling uncertainties. Simulation results reduce input dimensionality by one third and demonstrate close tracking of the desired trajectory in the presence of random perturbations.

II. Problem Formulation

A. n-Link Musculoskeletal Model

The problem must be formulated for synergy extraction and control. Consider an n-link model where element q_k ($k = 1, 2, \ldots, n$) of angular displacement vector $q \in R^n$ corresponds to the angle of the kth joint. Each joint is actuated by the flexors and extensors via FES and by an electric motor so that there are 3n actuators in total. The n-link model dynamics is

$$M(q)\ddot{q} + C(q,\dot{q})\dot{q} + G(q) + F(q,\dot{q}) + d(t) = \Gamma(t), \quad (1)$$

where $M \in R^{n\times n}$ is the inertia matrix, $C \in R^{n\times n}$ is the Coriolis matrix, $G \in R^n$ is the gravitational vector, $F \in R^n$ is the passive torque vector described in [27], $d \in R^n$ is the torque due to unmodeled disturbances, and $\Gamma \in R^n$ is the torque from motor and FES inputs.

The active torque is given by

$$\Gamma(t) = B(q,\dot{q},\mu)a(t), \quad (2)$$

where $a \in R^{3n}$ is the activation signal vector and $B \in R^{n\times 3n}$ is defined as $B = b(q,\dot{q})\mu$. $\mu \in R^{3n\times 3n}$ is the matrix of fatigue states, and the control scaling matrix $b(q,\dot{q}) \in R^{n\times 3n}$ is given as follows:

$$b = \begin{bmatrix} \psi_{1_f} & -\psi_{1_e} & \kappa_1 & \ldots & 0 & 0 & 0 \\ \vdots & \vdots & \vdots & \ddots & \vdots & \vdots & \vdots \\ 0 & 0 & 0 & \ldots & \psi_{n_f} & -\psi_{n_e} & \kappa_n \end{bmatrix}.$$

The elements $\psi_{k_j}(q_k,\dot{q}_k)$ are the bounded piecewise muscle force-length/force-velocity functions from [27]. Indices $j = f, e$ correspond to the flexors and extensors, respectively, and $j = m$ will henceforth correspond to the motors. The elements $\kappa_k \in R$ are the torque-current conversion constants. The fatigue matrix is given by $\mu = \mathrm{diag}([\mu_{1_f}, \mu_{1_e}, 1, \ldots, \mu_{n_f}, \mu_{n_e}, 1])$, and the muscle fatigue dynamics is

$$\dot{\mu}_{k_j} = T_{f_{k_j}}^{-1}(\mu_{min_{k_j}} - \mu_{k_j})a_{k_j} + T_{r_{k_j}}^{-1}(1-\mu_{k_j})(1-a_{k_j}), \quad (3)$$

for $j = f, e$ where $T_r, T_f \in R^+$ are the recovery and fatigue time constants, respectively, and $\mu_{min_{k_j}} \in (0,1)$ is the minimum fatigue value for muscle k_j.

Assumption 1: The disturbance d(t), desired joint trajectories $q_d(t)$, and their first and second time derivatives are bounded.

Assumption 2: The desired activation vector $a_d(t) \in R^{3n}$ and its first derivative are respectively bounded by known constants $a_{d_{max}}, \dot{a}_{d_{max}} \in R^+$.

B. Synergy-Inspired Decomposition

The activation vector a(t) is driven by a first-order dynamics as

$$\dot{a} = T_a^{-1}(u - a), \quad (4)$$

where $u(t) \in R^{3n}$ is the normalized input vector with elements $u_{k_j} \in [u_{min_{k_j}}, 1]$ and $T_a \in R^{3n\times 3n}$ is the diagonal matrix of activation time constants $T_{a_{k_j}} \in R^+$. Using an input dimensionality reduction method such as principal component analysis (PCA), a(t) can be decomposed into linear combinations of the actuators, or synergies, denoted

$$a = wc,$$

where $w \in R^{3n\times p}$ is a constant synergy weight matrix. The synergy activation vector $c(t) \in R^p$, $p < 3n$ can

be optimized in place of a(t) in order to reduce input dimensionality.

Assumption 3: Any loss of information during synergy decomposition of a is negligible.

Assumption 4: The terms in the synergy weight matrix w are bounded constants.

Using (4), the synergy activation dynamics is

$$\dot{c} = w^{\dagger} T_a^{-1}(u - wc),$$

where $[wc]_{k_j} \in [a_{min_{k_j}}, 1]$. Note that $a_{min_{k_j}}, u_{min_{k_j}} = 0$ for FES inputs and -1 for motor inputs.

C. Task-Space Model

Given the Jacobian $J(q) \in R^{2\times n}$ of the end effector and considering frontal and sagittal directions, the Cartesian endpoint velocity $\dot{z}(t) \in R^2$ is related to the joint velocity by $\dot{z} = J(q)\dot{q}$. The endpoint space dynamics is

$$M_z(z)\ddot{z} + C_z(z,\dot{z})\dot{z} + F_z(z,\dot{z}) + G_z(z) + d_z(t) = B_z(z,\dot{z},\mu)wc(t) \quad (5)$$

where $M_z = (J^T)^{\dagger} M J^{\dagger}$, $C_z = (J^T)^{\dagger}(C - MJ^{\dagger}\dot{J})J^{\dagger} \in R^{2\times 2}$, $G_z = (J^T)^{\dagger}G$, $F_z = (J^T)^{\dagger}F$, $d_z = (J^T)^{\dagger}d \in R^2$, and $B_z = (J^T)^{\dagger}B \in R^{2\times 3n}$.

Assumption 5: $J(q)$ is bounded by some $J_{max} \geq |J|$. Likewise, $J(q)^T$ is bounded by $J^{\dagger}_{max} \geq |J^T|$.

Property 1: M_z is positive definite and bounded by constants $\lambda_z, \lambda_Z \in R^+$ such that $\forall v \in R^2$, $\lambda_z||v||^2 \leq v^T M_z v \leq \lambda_Z||v||^2$.

Property 2: M_z and C_z are skew-symmetric, i.e., $v^T(\dot{M}_z - 2C_z)v = 0$, $\forall v \in R^2$.

D. Error Dynamics Development

The control objective of the MPC is to minimize error between a desired endpoint trajectory $z_d(t) \in R^2$ and the actual endpoint trajectory; thus, to formulate the MPC problem, the dynamics is first rewritten in terms of the state error. Let $e \in R^2$, the nominal position error, be given by

$$e = z_d - \bar{z},$$

where $\bar{z}(t) \in R^2$ is the nominal trajectory. Define the auxiliary error, $r \in R^2$, as

$$r = \dot{e} + \alpha e, \quad (6)$$

for constant gain $\alpha \in R^+$. The nominal error dynamics is

$$\bar{M}_z\dot{r} = \bar{M}_z(\ddot{z}_d + \alpha\dot{e}) + \bar{C}_z\dot{z} + \bar{F}_z + \bar{G}_z - \bar{B}_z wc. \quad (7)$$

Introduce an auxiliary function $N_d(z_d, \dot{z}_d, \ddot{z}_d) \in R^2$, defined as

$$N_d = M_z(z_d)\ddot{z}_d + C_z(z_d,\dot{z}_d)\dot{z}_d + F_z(z_d,\dot{z}_d) + G_z(z_d). \quad (8)$$

Given a desired dynamics $M_z(z_d)\ddot{z}_d + C_z(z_d,\dot{z})\dot{z}_d + F_z(z_d,\dot{z}_d) + G_z(z_d) = B_z(z_d,\dot{z}_d,\mu)a_d(t)$, the term $N_d(z_d,\dot{z}_d,\ddot{z}_d)$ can also be written as

$$N_d = B_z(z_d,\dot{z}_d,\mu_d)a_d(t), \quad (9)$$

where $\mu_d \in R^{6\times 6}$ is simply the identity matrix. By adding and subtracting N_d and $\bar{B}_z a_d$, (7) can be simplified as

$$\bar{M}_z\dot{r} = \tilde{N} - \bar{C}_z r - \tilde{B}a_d - \bar{B}_z wc + \bar{B}_z a_d - e, \quad (10)$$

where $\tilde{B} \in R^{2\times 3n}$ is $\tilde{B} = \bar{B}_z - B_z(z_d,\dot{z}_d,\mu_d)$ and $\tilde{N} \in R^2$ is $\tilde{N} = N - N_d$. Here, $N(z, z_d, \dot{z}, \dot{z}_d, \ddot{z})$ is defined as

$$N = \bar{M}_z\ddot{z}_d + \bar{C}_z(\dot{z}_d + \alpha e) + \bar{F}_z + \bar{G}_z + \bar{M}_z\alpha\dot{e} + e.$$

By the Mean Value Theorem and Assumptions 2 and 3, $\tilde{N}$ and $\tilde{B}a_d$ are bounded as

$$||\tilde{N}|| \leq \rho_1(||x_e||)||x_e||, \quad ||\tilde{B}a_d|| \leq \rho_2(||x_e||)||x_e||, \quad (11)$$

for class K functions $\rho_1, \rho_2 \in R^+$ and $x_e = [e^T\ r^T]^T \in R^4$.

1) Backstepping Error Dynamics: As the actual input, u, in (4) is cascaded to the actual dynamics in (5), we introduce a backstepping error $e_a \in R^{3n}$ as $e_a = wc - a_v$, where $a_v(t) \in R^{3n}$ is a virtual input to be designed. By adding and subtracting $\bar{B}_z a_v$, (10) becomes

$$\bar{M}_z\dot{r} = \tilde{N} - \bar{C}_z r - \tilde{B}a_d - \bar{B}_z e_a + \bar{B}_z a_d - \bar{B}_z a_v - e. \quad (12)$$

Defining the virtual input as $a_v = a_d + k_1\bar{B}_z^{\dagger} r$ for constant gain $k_1 \in R^+$, (12) becomes

$$\bar{M}_z\dot{r} = \tilde{N} - \bar{C}_z r - \tilde{B}a_d - \bar{B}_z e_a - k_1 r - e. \quad (13)$$

Using (4), the backstepping error dynamics is

$$\dot{e}_a = T_a^{-1} w(\bar{u}_{syn} - \bar{c}) - \dot{a}_v, \quad (14)$$

where the synergistic input $\bar{u}_{syn}(t) \in R^p$ is defined as $\bar{u}_{syn} = w^{\dagger}\bar{u}$. To obtain the optimal synergy coefficients, we define the control law for $\bar{u}_{syn}$ as

$$\bar{u}_{syn} = \bar{c} + w^{\dagger} T_a(\dot{a}_v + wv), \quad (15)$$

where $v(t) \in R^p$ is the synergistic input to be optimized by MPC. (14) reduces to

$$\dot{e}_a = wv. \quad (16)$$

Finally, collecting error dynamics in (6), (13), and (16), the state space equation is written as $\dot{\bar{x}} = f(\bar{x}, v)$, where $\bar{x} \in R^{3n+4}$ is $\bar{x} = [e^T\ r^T\ e_a^T]^T$ and $f(\bar{x}, v)$ is given by

$$f(\bar{x}, v) = \begin{bmatrix} r - \alpha e \\ \bar{M}_z^{-1}(\tilde{N} - \bar{C}_z r - \tilde{B}a_d - \bar{B}_z e_a - k_1 r - e) \\ wv \end{bmatrix}. \quad (17)$$

III. Robust MPC

A. Nominal MPC-based Optimization Scheme

The MPC problem can now be formulated using the running and terminal costs given by

$$l = \bar{x}^T Q\bar{x} + (wv)^T Rwv$$

$$V = \frac{1}{2}e^T e + \frac{1}{2}r^T\bar{M}_z r + \frac{1}{2}e_a^T e_a,$$

where $Q \in R^{(3n+4)\times(3n+4)}$, $R \in R^{3n\times 3n}$ are symmetric, positive definite weight matrices. Define $g_{k_j}(\bar{\mu}_{k_j}, \bar{a}_{k_j})$ as (3),

and let $[t_k, t_k+T]$ be the prediction horizon of constant length T. The optimization problem is posed as follows:

$$\min_{v(t)} J(\bar{x}(t), v(t)|t_k) = \int_{t_k}^{t_k+T} l\,dt + V(\bar{x}(t_k+T|t_k))$$

$$\text{s.t.} \quad \dot{\bar{x}} = f(\bar{x}, v)$$

$$\dot{\bar{\mu}}_{k_j} = g_{k_j}(\bar{\mu}_{k_j}, \bar{a}_{k_j}),\ j = f, e,\ \forall k$$

$$\bar{a}_{k_j} \in [a_{min_{k_j}}, 1],\ \forall j, k$$

$$\bar{\mu}_{k_j} \in [\mu_{min_{k_j}}, 1],\ \forall j, k$$

$$x_k \in \bar{x}(t_k|t_k) \in \Omega_\zeta \qquad wv \in U_{tube} \qquad \bar{x}(t_{k+T}|t_k) \in \Omega_\alpha$$

$$|(w\bar{c} + T_a\dot{a}_v)_{k_m}| \le 1 - U_F - (T_a\gamma)_{k_m},\ \forall k$$

$$(w\bar{c} + T_a\dot{a}_v)_{k_j} \le 1 - (T_a\gamma)_{k_j},\ j = f, e,\ \forall k$$

The final two constraints ensure that $u \le 1$ and $|u| \le 1$ for FES and motors, respectively. The terminal set Ω_α is

$$||\bar{x}(t_k+T|t_k)||^2 \le \frac{3n+4}{3n}\frac{||\gamma||^2}{k_2^2},$$

where $k_2 \in R^+$ and $\gamma \in R^{3n}$ is a vector of constants $\gamma_{k_j} \in R^+$ such that $|(wv)_{k_j}| \le \gamma_{k_j}, \forall k, j$. Ω_ζ is the tube region and is defined as $\Omega_\zeta = \{\zeta \mid ||\zeta|| \le \varepsilon\sqrt{1+\frac{1}{\beta^2\iota^2}}\sqrt{\lambda_z/\lambda_z} + 2\varepsilon\sqrt{\frac{1}{\lambda_z\lambda_z\iota^2}}\}$, where $\zeta = [\epsilon^T\ \dot{\epsilon}^T]^T$, $\iota \in (0,1)$, and $\lambda_z, \lambda_z \in R^+$ are the constants from Property 1. The control boundary U_{tube} constrains the nominal inputs and is defined as

$$||wv||^2 \le ||\gamma||^2.$$

B. Sliding Mode Controller

In this subsection, we design a sliding mode controller (SMC) based on [28] that acts as a tube to provide robustness to the nominal MPC scheme. Let $\tau_{fz}, \tau_{mz} \in R^2$ be the task-space torques generated by FES and motors, respectively. To account for the disturbance $d_z(t)$, introduce SMC torque $\gamma_{Fz} = (\tau_{mz} - \bar{\tau}_{mz}) \in R^2$. The dynamics can be rewritten as

$$M_z\ddot{z} + C_z\dot{z} + F_z + G_z + d_z = \gamma_{Fz} + \tau_{fz} + \bar{\tau}_{mz}.$$

Let $z(t) \in R^2$ be the true endpoint. Next, introduce the position error term $\epsilon \in R^2$ as $\epsilon = \bar{z} - z$ and the auxiliary error $\delta \in R^2$ as

$$\delta = \dot{\epsilon} + \beta\epsilon$$

for constant gain $\beta \in R^+$. Let $\bar{\tau}_{fz}$ be the nominal FES torque. The error dynamics is

$$M_z\dot{\delta} = M_z(\ddot{\epsilon} + \beta\dot{\epsilon}) - \tau_{mz} - \tau_{fz} + C_z\dot{z} + F_z + G_z + d_z \tag{18}$$

Introduce auxiliary functions $P(z, \bar{z}, \dot{z}, \dot{\bar{z}}, \ddot{\bar{z}}), \bar{P}(\bar{z}, \dot{\bar{z}}) \in R^2$ as

$$P = M_z\ddot{\bar{z}} + C_z(\dot{\bar{z}} + \beta\epsilon) + F_z + G_z - \tau_{fz} + M_z\beta\dot{\epsilon}$$

$$\bar{P} = \bar{M}_z\ddot{\bar{z}} + \bar{C}_z\dot{\bar{z}} + \bar{F}_z + \bar{G}_z - \bar{\tau}_{fz},$$

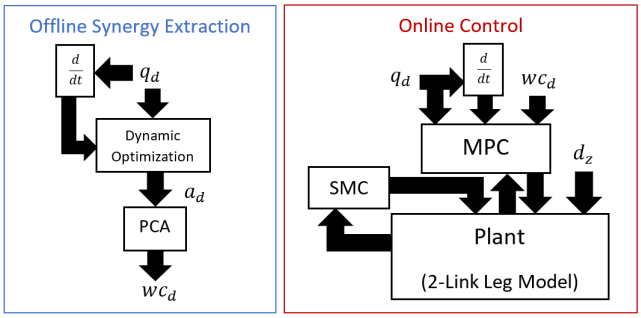

Figure 1. High-level control diagram.

and define $\tilde{P} \in R^2$ as $\tilde{P} = P - \bar{P}$. (18) reduces to

$$M_z\dot{\delta} = \tilde{P} - C_z\delta + d_z - \gamma_{Fz}. \tag{19}$$

Because μ_{k_j} and $(wc)_k$ are bounded, normalized variables, it is true that $||\bar{\tau}_f(\bar{q}, \dot{\bar{q}}, \bar{\mu}, w\bar{c})||_k \le ||\psi_{k_f}(\bar{q}, \dot{\bar{q}})|| + ||\psi_k(\bar{q}, \dot{\bar{q}})||$. By Assumption 5, $\bar{\tau}_{fz}$ is also bounded, so $\tilde{P}$ must be bounded by class K function $\rho_3 : R^+ \to R^+$ such that $||\tilde{P}|| \le \rho_3(||\sigma||)||\sigma||$, where $\sigma = [\epsilon^T\ \delta^T]^T \in R^4$. The SMC torque is thus designed as

$$\gamma_{Fz} = \rho_3(||\sigma||)||\sigma||\text{sat}(\frac{\delta}{\varepsilon}) + \bar{d}\,\text{sat}(\frac{\delta}{\varepsilon}) + \kappa_f\delta, \tag{20}$$

for constant gain $\kappa_f \in R^+$. $\bar{d} \in R^+$ is chosen such that $||d_z(t)||_2 \le \bar{d}, \forall t$. For known constant $\varepsilon \in R^+$, the saturation vector $\text{sat}(\frac{\delta}{\epsilon}) \in R^2$ is

$$\text{sat}(\frac{\delta}{\varepsilon}) = \begin{cases} \frac{\delta}{||\delta||}, & ||\delta|| \ge \varepsilon \\ \frac{\delta}{\varepsilon}, & ||\delta|| < \varepsilon \end{cases}$$

Assumption 6: The SMC activation may be approximated as the SMC input, i.e., $u_{Fz} \approx a_{Fz}$.

Given that ρ_3, σ, and δ are bounded (see Section IV-C), the SMC torque is bounded as

$$||\gamma_{Fz}|| \le \Omega_\rho\Omega_\sigma + \bar{d} + \kappa_f\Omega_\delta. \tag{21}$$

IV. Stability Analysis

A. Terminal State Invariance and Asymptotic Stability

Lemma 1. If the terminal control input is chosen as $v_T = -k_2w^+e_a$ for positive constant gain k_2, then control gains α, k_1,and k_2 and weight matrices Q and R can be chosen such that the terminal state is invariant and the nominal system is asymptotically stable (AS).

Proof: The control gains, terminal controller, and terminal region can be designed such that $\dot{V} + l \le 0$ and the terminal state is invariant. Invoking Property 2, $\dot{V}$ is given by

$$\dot{V} = -\alpha||e||^2 + r^T(\tilde{N} - \tilde{B}\bar{a}_d - \bar{B}_z e_a) - k_1||r||^2 + e_a^T wv. \tag{22}$$

Defining the terminal control input as $v_T = -k_2w^+e_a \in R^p$ for constant $k_2 \in R^+$ and recalling (11), (22) is bounded as

$$\dot{V} \le -\alpha||e||^2 + \bar{\rho}(||x_e||)||\bar{x}||^2 - r^T\bar{B}_z e_a - k_1||r||^2 - k_2||e_a||^2,$$

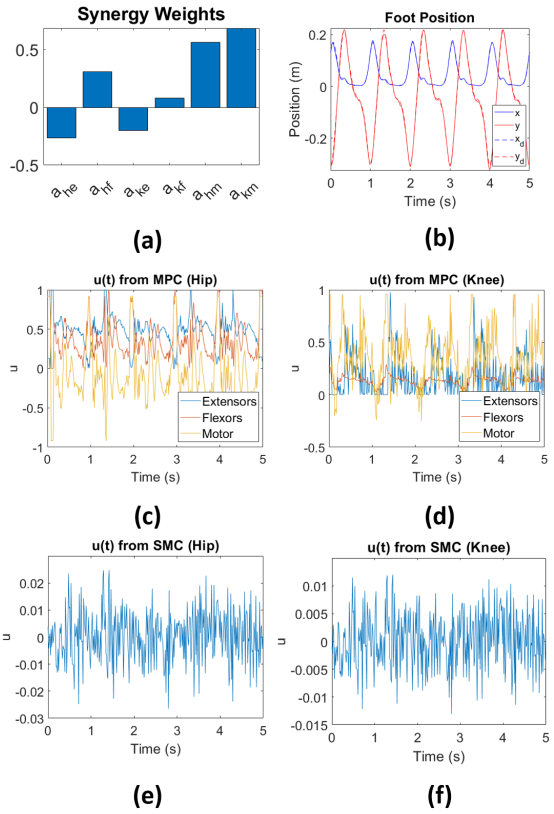

Figure 2. (a) Weights for the most dominant extracted synergy. (b) Foot trajectory tracking with TMPC. a_{he} represents hip extensor activation, and likewise for the other 5 actuators. Also depicted are the MPC inputs for hip (c) and knee (d) actuators as well as the SMC inputs for hip (e) and knee (f) motors.

where $\bar{\rho} = \rho_1 + \rho_2$. Since $\bar{\mu}_{k_j} \in [0,1]$ and $\bar{b}$ consists of bounded functions $\bar{\psi}_{k_j}$ and constants κ_k, and by Assumption 5, there must be some constant $B_{max} \in \mathbb{R}^+$ such that $|B_z| \leq B_{max}$. Hence,

$$\dot{V} \leq -(K_{min} - \bar{\rho}(||x_e||) - B_{max})||\bar{x}||^2,$$

where $K_{min} \in \mathbb{R}^+$ is $K_{min} = \min\{\alpha, k_1, k_2\}$. As long as $\rho(||x_e||) + B_{max} < K_{min}$, which is true when $||x_e|| < \bar{\rho}^{-1}(K_{min} - B_{max})$, it follows that $\dot{V} < 0$. Thus, the terminal state is invariant. Let $Q = diag(q_1, \ldots, q_{3n+4})$ and $R = diag(p_1, \ldots, p_{3n})$, and let $q_e = \max(q_1, q_2)$, $q_r = \max(q_3, q_4)$, $q_a = \max(q_5, \ldots, q_{3n+4})$, and $\tilde{p} = \max(p_1, \ldots, p_{3n})$. l is thus bounded as

$$l \leq q_e||e||^2 + q_r||r||^2 + (q_a + \tilde{p}k^2)||e_a||^2,$$

and it is therefore true that

$$\dot{V} + l \leq -(K_{min} - \bar{\rho}(||x_e||) - B_{max} - K_{max})||\bar{x}||^2,$$

where $K_{max} \in \mathbb{R}^+$ is $K_{max} = \max\{q_e, q_r, q_x + \tilde{p}k^2\}$. As long as $K_{min} > \bar{\rho}(||x_e||) + B_{max} + K_{max}$, it is true that $\dot{V} + l < 0$, and the nominal system is AS. ■

B. Recursive Feasibility

Theorem 2. If $\xi \in \mathbb{R}^+$ is the maximum possible error magnitude for all $\bar{x}_{k_j}$, then the nominal system is recursively feasible as long as $\xi \leq \frac{||y||}{k_2\sqrt{3^n}}$.

Proof. Available upon request.

C. Uniform Ultimate Boundedness

Theorem 3. The SMC torque $\gamma_{Fz} \in \Gamma_{Fz}$ ensures the system in (19) is uniformly ultimately bounded (UUB) such that σ exponentially enters an invariant set Ω_σ and $u_F(t) \in \mathbb{R}^n$, the SMC input in joint space, is bounded as $U_F = \{u_F \mid ||u_F|| \leq \kappa_{min}^{-1} J_{max}^{\dagger}(\Omega_\rho\Omega_\sigma + \bar{d} + \kappa_f\Omega_\delta)\}$, where $\kappa_{min} = \min\{|\kappa_1|, \ldots, |\kappa_n|\}$ and $\Omega_\delta, \Omega_\rho$ are invariant sets bounding δ and ρ_3, respectively.

Proof. Available upon request.

D. Input Constraints

Lemma 2. If $|(w\bar{c} + T_a\dot{a}_v)_{k_m}| \leq 1 - U_F - T_a\gamma_{k_m}, \forall k$, then the motor constraint $u_{k_m} \in [-1, 1]$ is satisfied.

Proof. Available upon request.

Lemma 3. If $(w\bar{c} + T_a\dot{a}_v)_{k_j} \leq 1 - (T_a\gamma)_{k_j}, j = f, e, \forall k,$, then the FES constraint $u_{k_j} \leq 1$ is satisfied.

Proof. Available upon request.

V. Simulation Results

The TMPC was implemented on a 2-link leg model with parameters from [27], [29], [30]. The model possessed bidirectional hip and knee motors and FES-actuated hip extensors, hip flexors, knee extensors, and knee flexors. The desired "foot" (the distal endpoint of the shank) trajectory was calculated from the walking-like trajectories employed in [29]. Defining $\tilde{q} = [q^T \quad \dot{q}^T]^T$ and $f_q = [\dot{q}^T \quad M^{-1}(Ba - C\dot{q} - F - G)^T]^T$, desired activations were extracted through dynamic optimization with the following MPC scheme:

$$\min_{a(t)} \quad J(\tilde{q}(t), a(t) \mid t_k) = \int_{t_k}^{t_{k+T}} e_q(t)\tilde{Q}e_q(t)\,dt$$
$$\text{s.t.} \quad \dot{\tilde{q}} = f_q(\tilde{q}, a)$$
$$a_{k_j} \in [a_{min_{k_j}}, 1], \forall k, j$$

where joint-space error $e_q \in \mathbb{R}^2$ is $e_q = q_d - q$ and $\tilde{Q} \in \mathbb{R}^{2\times 2}$ is a symmetric, positive definite weight matrix. The symbolic optimization framework CasADi was used for the MPC. PCA was performed in MATLAB R2019a to identify synergy weights from optimal activations. It was found that 4 synergies accounted for 99.97% of the variance. A high-level diagram of the synergy extraction and simulations can be seen in Fig. 1, and the weights for the most dominant synergy are displayed in Fig. 2 (a).

The TMPC was performed with CasADi in MATLAB R2019a using the 4 most dominant synergies and a 0.0145s timestep. Simulations were run for 5s to complete 5 cycles with random joint position and velocity perturbations

(0.01rad, 0.01rad/s, ∀i) applied at each iteration. The average root-mean-square error (RMSE) in foot position across 10 simulations was 0.27 and 0.83cm in the vertical (x) and horizontal (y) directions, respectively. Example tracking performance of the controller is shown in Fig. 2 (b), and the MPC and SMC inputs are displayed in Fig. 2 (c)-(f). Note that the first 3 curves in Fig. 2 (c) and (d) are elements of $\bar{u} = w\bar{u}_{syn}$. As expected, the input magnitude from the SMC is smaller than that from the MPC.

VI. Conclusion and Future work

A TMPC framework was designed in task space to optimize synergy activations for n-link HN with n motor and 2n FES actuators. The framework included activation and fatigue dynamics, and stability and recursive feasibility were proven. The TMPC was implemented on a 2-DOF model with hip and knee actuation. The controller tracked the desired trajectory for a walking-like motion even though the synergy paradigm reduced the number of actuators by one third. Future work will extend synergistic TMPC to include ankle actuation for implementation in HN walking experiments. Furthermore, it is desirable to incorporate step planning into the controller so that the controller both plans and executes the desired trajectory. Lastly, FES-induced muscle fatigue feedback can be incorporated for modulating or switching synergies to promote muscle recovery.

References

[1] NSCISC, "Spinal cord injury facts and figures at a glance," National Spinal Cord Injury Statistical Center: Birmingham, AL., 2020.

[2] L. Giangregorio and N. McCartney, "Bone loss and muscle atrophy in spinal cord injury: epidemiology, fracture prediction, and rehabilitation strategies," The journal of spinal cord medicine, vol. 29, no. 5, pp. 489–500, 2006.

[3] A. E. Scremin, L. Kurta, A. Gentili, B. Wiseman, K. Perell, C. Kunkel, and O. U. Scremin, "Increasing muscle mass in spinal cord injured persons with a functional electrical stimulation exercise program," Archives of physical medicine and rehabilitation, vol. 80, no. 12, pp. 1531–1536, 1999.

[4] M. Bélanger, R. B. Stein, G. D. Wheeler, T. Gordon, and B. Leduc, "Electrical stimulation: can it increase muscle strength and reverse osteopenia in spinal cord injured individuals?" Archives of physical medicine and rehabilitation, vol. 81, no. 8, pp. 1090–1098, 2000.

[5] S.-C. Chen, C.-H. Lai, W. P. Chan, M.-H. Huang, H.-W. Tsai, and J.-J. J. Chen, "Increases in bone mineral density after functional electrical stimulation cycling exercises in spinal cord injured patients," Disability and Rehabilitation, vol. 27, no. 22, pp. 1337–1341, 2005.

[6] T. Street and C. Singleton, "A clinically meaningful training effect in walking speed using functional electrical stimulation for motor-incomplete spinal cord injury," The Journal of Spinal Cord Medicine, vol. 41, no. 3, pp. 361–366, 2018.

[7] B. C. Craven, L. M. Giangregorio, S. M. Alavinia, L. A. Blencowe, N. Desai, S. L. Hitzig, K. Masani, and M. R. Popovic, "Evaluating the efficacy of functional electrical stimulation therapy assisted walking after chronic motor incomplete spinal cord injury: effects on bone biomarkers and bone strength," The journal of spinal cord medicine, vol. 40, no. 6, pp. 748–758, 2017.

[8] B. M. Doucet, A. Lam, and L. Griffin, "Neuromuscular electrical stimulation for skeletal muscle function," The Yale journal of biology and medicine, vol. 85, no. 2, p. 201, 2012.

[9] A. Stewart, C. Pretty, and X. Chen, "A portable assist-as-need upper-extremity hybrid exoskeleton for FES-induced muscle fatigue reduction in stroke rehabilitation," BMC Biomedical Engineering, vol. 1, no. 1, pp. 1–17, 2019.

[10] K. H. Ha, S. A. Murray, and M. Goldfarb, "An approach for the cooperative control of FES with a powered exoskeleton during level walking for persons with paraplegia," IEEE Transactions on Neural Systems and Rehabilitation Engineering, vol. 24, no. 4, pp. 455–466, 2015.

[11] A. Ekelem and M. Goldfarb, "Supplemental stimulation improves swing phase kinematics during exoskeleton assisted gait of sci subjects with severe muscle spasticity," Frontiers in neuroscience, vol. 12, p. 374, 2018.

[12] M. Rastegar and H. R. Kobravi, "A hybrid-FES based control system for knee joint movement control," Basic and Clinical Neuroscience, vol. 12, no. 4, pp. 441–452, 2021.

[13] E. Bardi, S. Dalla Gasperina, A. Pedrocchi, and E. Ambrosini, "Adaptive cooperative control for hybrid FES-robotic upper limb devices: a simulation study," in 2021 43rd Annual International Conference of the IEEE Engineering in Medicine & Biology Society (EMBC). IEEE, 2021, pp. 6398–6401.

[14] P. Müller, A. J. Del Ama, J. C. Moreno, and T. Schauer, "Adaptive multichannel FES neuroprosthesis with learning control and automatic gait assessment," Journal of neuroengineering and rehabilitation, vol. 17, no. 1, pp. 1–20, 2020.

[15] B. Sijobert, C. Azevedo, J. Pontier, S. Graf, and C. Fattal, "A sensor-based multichannel FES system to control knee joint and reduce stance phase asymmetry in post-stroke gait," Sensors, vol. 21, no. 6, p. 2134, 2021.

[16] M. A. Alouane, W. Huo, H. Rifai, Y. Amirat, and S. Mohammed, "Hybrid FES-exoskeleton controller to assist sit-to-stand movement," IFAC-PapersOnLine, vol. 51, no. 34, pp. 296–301, 2019.

[17] M. Nandor, R. Kobetic, M. Audu, R. Triolo, and R. Quinn, "A muscle-first, electromechanical hybrid gait restoration system in people with spinal cord injury," Frontiers in Robotics and AI, vol. 8, 2021.

[18] N. A. Kirsch, X. Bao, N. A. Alibeji, B. E. Dicianno, and N. Sharma, "Model-based dynamic control allocation in a hybrid neuroprosthesis," IEEE Transactions on Neural Systems and Rehabilitation Engineering, vol. 26, no. 1, pp. 224–232, 2017.

[19] N. Kirsch, N. Alibeji, and N. Sharma, "Nonlinear model predictive control of functional electrical stimulation," Control Engineering Practice, vol. 58, pp. 319–331, 2017.

[20] X. Bao, Z. Sheng, B. E. Dicianno, and N. Sharma, "A tube-based model predictive control method to regulate a knee joint with functional electrical stimulation and electric motor assist," IEEE Transactions on Control Systems Technology, vol. 29, no. 5, pp. 2180–2191, 2020.

[21] Z. Sun, X. Bao, Q. Zhang, K. Lambeth, and N. Sharma, "A tube-based model predictive control method for joint angle tracking with functional electrical stimulation and an electric motor assist," in 2021 American Control Conference (ACC). IEEE, 2021, pp. 1390–1395.

[22] M. C. Tresch, P. Saltiel, and E. Bizzi, "The construction of movement by the spinal cord," Nature neuroscience, vol. 2, no. 2, pp. 162–167, 1999.

[23] T. Bajd, A. Kralj, R. Turk, H. Benko, and J. Šega, "The use of a four-channel electrical stimulator as an ambulatory aid for paraplegic patients," Physical Therapy, vol. 63, no. 7, pp. 1116–1120, 1983.

[24] N. A. Alibeji, V. Molazadeh, F. Moore-Clingenpeel, and N. Sharma, "A muscle synergy-inspired control design to coordinate functional electrical stimulation and a powered exoskeleton: artificial generation of synergies to reduce input dimensionality," IEEE Control Systems Magazine, vol. 38, no. 6, pp. 35–60, 2018.

[25] A. Ahmad, "Variable step length control for a hybrid neuroprosthesis using dynamic movement primitives and model predictive control," Master's thesis, University of Pittsburgh, 2021.

[26] S. Maggioni, N. Reinert, L. Lünenburger, and A. Melendez-Calderon, "An adaptive and hybrid end-point/joint impedance controller for lower limb exoskeletons," Frontiers in Robotics and AI, vol. 5, no. 104, 2018.

[27] D. Popovic, R. B. Stein, M. N. Oguztoreli, M. Lebiedowska, and S. Jonic, "Optimal control of walking with functional electrical stimulation: a computer simulation study," IEEE Transactions on Rehabilitation Engineering, vol. 7, no. 1, pp. 69–79, 1999.

[28] H. Khalil, "Nonlinear design tools," Nonlinear systems, pp. 551–625, 2002.

[29] N. Alibeji, N. Kirsch, and N. Sharma, "An adaptive low-dimensional control to compensate for actuator redundancy and FES-induced muscle fatigue in a hybrid neuroprosthesis," Control Engineering Practice, vol. 59, pp. 204–219, 2017.

[30] R. Drillis, R. Contini, and M. Bluestein, "Body segment parameters," Artificial limbs, vol. 8, no. 1, pp. 44–66, 1964.